Pharmaceutical Research, Vol. 25, No. 6, June 2008 (© 2007)
DOI: 10.1007/s11095-007-9530-y

Research Paper

Application of Calorimetry, Sub-Ambient Atomic Force Microscopy and Dynamic Mechanical Analysis to the Study of Frozen Aqueous Trehalose Solutions

Jiejun Wu,[1] Mike Reading,[1,2] and Duncan Q. M. Craig[1]

Received October 2, 2007; accepted December 20, 2007; published online February 7, 2008

Purpose. Disaccharides such as trehalose are widely used as cryo-protectants to maintain the activity of proteinaceous drugs during freezing. One unresolved issue is the double transition that is observed very commonly in DSC experiments on disaccharide solutions in the frozen state; the assignment of these transitions remains disputed. Here we use calorimetry and two new techniques to shed light on the true nature of these transitions.
Methods. Modulated Temperature DSC (MTDSC), cryo atomic force microscopy (AFM) and a novel DMA technique were used to study these transitions.
Results. MTDSC identified the two transitions Tr_1 and Tr_2 at −35.4 and −27.9°C respectively in the reversing heat flow signal, an exotherm and endotherm were observed in the non-reversing signal at circa −32 and −29°C respectively. It is shown for the first time that AFM images can be obtained of a softening and melting sample without damaging it. A force modulation imaging technique showed a softening at Tr_1 and a loss of ice crystals at Tr_2. These observations were supported by the DMA results.
Conclusions. The results indicate Tr_1 is associated with a glass transition while Tr_2 is associated with the onset of loss of crystallinity.

KEY WORDS: atomic force microscopy; freezing; microthermal analysis; modulated temperature differential scanning calorimetry; trehalose.

INTRODUCTION

The process of freeze drying is of increasing importance within the pharmaceutical industry. However, this process can generate a range of stresses on biomolecules or tissues due to both the freezing and subsequent water removal steps. In order to increase the tolerance of the material in question to those stresses, various additives such as sugars and polyols are widely used, particularly as a means of stabilizing pharmaceutical preparations for which freeze drying would otherwise result in extensive drug degradation. The various sugars or polyols have differing stabilization abilities; disaccharides appear to be the particularly effective (1,2) with trehalose attracting considerable interest due to clear evidence for it protecting the activity of complex biomolecules such as proteinaceous drugs (3).

Despite the widespread use of these cryo- and lyoprotectants, the mechanisms associated with the preservation process are still unclear, with numerous hypotheses having been presented to explain and predict preservation efficiency (4–10). Similarly, it is also essential to establish the optimum conditions for the freeze drying process in order to prevent phenomena such as collapse (11) which occurs when the primary drying process takes place at a temperature significantly higher than the glass transition temperature (T_g). In brief, the collapse temperature is generally considered to be a few degrees above T_g, hence measurement of the T_g represents a powerful predictive tool to prevent product failure. One widely studied approach is to examine the thermal properties of the frozen aqueous solutions using differential scanning calorimetry (DSC). However, this analysis is complicated by the appearance of a double transition which is very commonly observed in disaccharide solutions in the frozen state; there is still no universal agreement on the assignment of these transitions (12–20). The lower transition (Tr_1) is generally believed to be the 'true' glass while the higher transition (Tr_2) has been ascribed to the onset of ice crystals dissolving (12,13), this view was described by Ablett *et al.* (13) and this has become, broadly speaking, the consensus amongst most workers in the field. However, it has also been interpreted in terms of the presence of the solute inclusions (17), an interfacial interaction between ice crystal and the amorphous phase (19) and, recently, it has been suggested that Tr_2 is also a 'true' glass transition (20). These contradictory conclusions point to the need to use other techniques in addition to calorimetry as the extensive calorimetric work to date has not enabled a clear conclusion to be reached. A better understanding of the nature of these double transitions would have considerable benefits in terms

[1] School of Chemical Sciences and Pharmacy, University of East Anglia, Norwich, Norfolk, NR4 7TJ, UK.
[2] To whom correspondence should be addressed. (e-mail: mike.reading@uea.ac.uk)

of protocol design, particularly given the well known relationship between cost and drying temperature which necessitates the use of the highest temperature without causing collapse (21).

In this investigation we have used three techniques; modulated temperature DSC (MTDSC), low temperature atomic force microscopy (AFM) and dynamic mechanical analysis (DMA). The latter two have limited or no use in the field of frozen aqueous systems. With regard to MTDSC, this is now an established technique and the reader is referred to refs. (22–24) for further information.

Atomic force microscopy (AFM) is now also a well established technique (25) and the basic details of its operation will not be discussed here. However, we present a novel application for the method in terms of sub-ambient imaging of a frozen system as it traverses temperature ranges over which transitions occur while avoiding significant damage to the sample. Here we use the instrument in contact mode, where the force applied by the tip to the sample is held constant, and in force modulation mode where the force is modulated sinusoidally while maintaining contact with the surface. The amplitude of the resistance to the force modulation, as measured by the bending of the cantilever, is a measure of the stiffness of the material immediately beneath the tip. In terms of temperature control, heated stage AFM is now well established but sub-ambient (lower than −40°C) studies are less so. Nevertheless, low temperatures have been achieved in order to image biomolecules such as antibodies, DNA or proteins, where the low temperatures eliminate molecular motion (26). A significant disadvantage of these approaches is that most such systems can only be operated in high vacuum (27). In our case, where we are seeking to study frozen aqueous systems, vacuum is not appropriate as it will lead to the sample freeze drying (an interesting topic for study in its own right but not the subject we are addressing here). Frozen systems have been imaged using AFM at atmospheric pressure by immersing the sample in a barrier fluid such as ethanol (28). This creates its own difficulties as the barrier fluid may change the way both the sample and cantilever behave, particularly when using imaging modes that involve rapid movement of the probe such as the force modulation mode we used in this work. Shao *et al.* (29–30) and Yamamoto *et al.* (31) have reported low temperature imaging at atmospheric pressure with a custom built AFM located entirely within a Dewar containing liquid nitrogen. They demonstrated imaging of a frozen aqueous surface at −150°C in contact mode (although some damage was observed, see ref. (31)). In contrast our objective was to image at higher temperatures while the sample was undergoing transitions that involved a softening of the sample surface and structural changes, without causing significant damage with the probe tip. We believe that we demonstrate this capability for the first time in this study.

We have used a novel stage, designed by Reading and Kamp (the latter is from the company Linkam Scientific Instruments Surrey, UK), which enables imaging at atmospheric pressure under nitrogen down to temperature as low as −70°C. This is achieved by flooding the area around the sample with dry nitrogen that is derived from the liquid nitrogen reservoir used to cool the sample (and which is, therefore, moisture free). The sample area is encased in a small cowl that has a slot in the top to allow the probe to access the sample surface. This simple arrangement allows the sample to be cooled without water condensing onto its surface and probe. It also means that the AFM can be used without modification and with all of the usual imaging modes being available.

DMA is a widely used method for studying polymers (32) and so the details of the technique will not be discussed here. Some work has been done on DMA of frozen sucrose systems using a specially designed sample holder (33). We used a novel experimental approach that allowed frozen systems to be studied in a DSC pan; we placed the sample in a hermetically sealed aluminium pan, care was taken to ensure the crucible was completely filled by the sample with no air gap. The pan was then placed beneath the DMA probe in a configuration akin to compression mode. The sample was rapidly cooled and the modulation of the probe position was started once the sample achieved the minimum set temperature. An advantage of this approach was that, in addition to the information on dynamic modulus, the probe position gave information on the thickness of the pan-sample composite thus the expansion and contraction of the sample could be detected. Using this method also ensured that the conditions experienced by the sample in the DMA would be very similar to that in the DSC.

We have therefore used MTDSC, cryo-mode AFM and DMA in conjunction to identify the transitions for a frozen aqueous trehalose system and to correlate those transitions with changes in surface topography and mechanical properties, thereby for the first time allowing the relationship between Tr_1 and Tr_2 and the surface and mechanical properties of the frozen system to be correlated.

MATERIALS AND METHODS

Materials and Sample Preparation

D-(+)-trehalose dihydrate (Hayashibara, Japan, purity not less than 99.0%) was used without further purification. Trehalose solution 200 mg/ml was prepared in ultra pure water. Solutions were allowed to equilibrate for 12 h and passed through a 0.22 μm filter before being used.

Thermal Analysis by MTDSC

MTDSC studies were performed using a TA 2920 MDSC (TA Instruments, Leatherhead, UK). A sample size of 15 or 2 μl on a piece of fresh peeled mica was used with nitrogen gas as the carrier gas for all experiments. Matched hermetic pans with 50 μm pinholes from Perkin Elmer were used for all runs. It was established that such small holes did not lead to any measurable weight loss in this experiment but did prevent the pan changing shape as a consequence of changing pressure with temperature. A full calibration was carried out using an underlying heating rate of 2°C/min with ±1°C amplitude and 60 s period. Temperature calibration was performed using *n*-octadecane (99.9%, Riedel-de-Hahn AG, Germany, theoretical melting point 28.24°C), Cyclohexane (99.9%, Riedel-de-Hahn AG, Germany, theoretical melting point 6.54°C) and *n*-decane (99+%, Sigma-Aldrich, Germany, theoretical melting point −29.7°C). Cell constant calibration

was used by *n*-decane as well. Heat capacity constant calibration was performed using aluminium oxide (100 mesh, 99.9%, Aldrich Chemical Co.,WI, USA). The sample was fast cooled (i.e. 'crash' cooling corresponding to some tens of degrees per minute) to −60°C then heated (with no annealing) at 2°C/min with ±1°C modulation amplitude and 60 s period.

AFM and Thermal Probe Studies

An Explorer AFM system made by the company Topometrix was combined with a cold stage (described in a previous section) was applied to image the frozen trehalose solution. A fresh piece of peeled mica on which was placed a small volume of sample solution (2 μl) was loaded onto the stage in room temperature and rapidly cooled down to −60°C then imaged over the relevant temperature range in contact mode or force modulation mode. During modulated force data acquisition, a 1:1 scan range to scan rate ratio (e.g. a 100 μm scan range at 100 μm/s), amplitude 15 Å and three cycles averaging were used.

A problem that was encountered early in this project was that the commonly used silicon probes damaged the surface even when used in tapping or pulsed force modes. There was also the problem that it was difficult to be sure of the temperature at the tip as it is reasonable to assume that the heat would be conducted from the AFM probe holder along the probe to the tip, thus the temperature at the point of contact would be different from the rest of the sample and that of the stage. Both of these problems were resolved by using ultra high compliance polyimide thermal probes made by Picocal (34) (Picocal Inc., USA); they could be used to measure the surface temperature and it was found that they could also be used in contact mode without damaging the sample. The disadvantage of these probes is that the larger radius of curvature of the tip (approx. 100 nm compared to 10 nm for a silicon AFM probe, this is further discussed below) means that the spatial resolution is much lower than conventional AFM. However, the spatial resolution is perfectly adequate to make a number of important observations. The tip height was 8 μm, the nominal spring constant was 0.1 N/m, length 393 μm with width 214 μm and thickness 3 μm. The cantilever material was polyimide with an embedded thin wire of Cr/Au. A surface temperature calibration was necessary to account for the temperature error between the cold stage and sample surface. A series of experiments were carried out in which the probe was placed on the bare surface of the stage. This has a calibrated embedded platinum resistance thermometer close to the surface. The accuracy of the temperature calibration was confirmed using *N*-octadecane (28.24°C), cyclohexane (6.54°C), water (0°C) and *n*-decane, (−29.7°C) all of which melted at the correct temperatures as observed by visual inspection using the optical microscope that is part of the AFM. The electrical resistance of the probe was measured as a function of temperature. In a second series of experiments the same measurement was made on the surface of a sample deposited on Mica. The temperature, as measured by the probe resistance, was found to be only a ±0.2°C different from the stage temperature even at the lowest value used in this study. Consequently the temperatures given in the AFM images are that of the stage.

Mechanical Properties Studies by DMA

Dynamic Mechanical Analysis (DMA 2980, TA Instrument) was used to measure changes in mechanical properties with temperature. A blade typically employed for three-point-bend measurements was used in this experiment. The sample was carefully sealed into a hermetic aluminium DSC pan without air gap then placed underneath the probe in the DMA. The temperature was fast cooled to −60°C (i.e. 'crash' cooling corresponding to some tens of degrees per minute) then increased to 0°C at 2°C/min. A static force of 6 N and a modulation amplitude of 10 μm was applied at 1 Hz during heating. Because this is a non-standard configuration the measurements of modulus could not be quantitative but tan delta and probe displacement (the average position of the probe) are not affected by this.

RESULTS

Figure 1 shows the MTDSC response for the frozen trehalose solution; both a 'conventional sample' simply loaded into a pan in the usual way and a sample on mica to imitate the conditions of the AFM experiments. MTDSC provides the same information as conventional DSC, the total heat flow signal, and also allows separation of the reversing and non-reversing components that constitute this response. The reversing component will show a step change at a glass transition and, typically, a peak during melting. In Fig. 1, the two samples both have very similar total heat flows and show two step-like transitions in the reversing signals that are characteristic of frozen sugar solutions with inflection points at about −35 and −28°C with the higher temperature transition being located at or close to the onset of a peak that can be ascribed to crystalline order being lost. The non-reversing heat flows are also shown, both samples exhibiting a small exotherm (circa −32°C) prior to an endotherm at (circa −29°C). Because the results from the two samples are very similar we conclude that the AFM results on mica can be considered to be representative of the bulk behaviour normally studied by DSC. It should be noted that these cooling conditions meant that the glass was not maximally concentrated, this is clearly evidenced by the exotherm which result from crystallisation. Maximal concentration is usually achieved by annealing and this was not used in this study. The results of a separate study on annealing will be the subject of a future article.

Before presenting the AFM results it is appropriate to discuss some aspects of these experiments; as the sample was frozen its surface became visibly rough as seen by the optical microscope that is part of the AFM. It seems clear that this was because of the formation of ice crystals. The z axis travel of the AFM is 10 μm maximum and so areas with features higher than this could not be imaged. It was found that images could be obtained of smoother areas only (in Fig. 2 the z range goes up to nearly 8 μm) thus the AFM images are necessarily of populations of the smaller crystals that were formed. It was also observed using the optical microscope that the rougher areas, i.e. those containing larger ice crystals, changed in appearance at higher temperatures than the smoother areas. This suggested that the AFM images that were obtained were of areas that contained the fraction of the

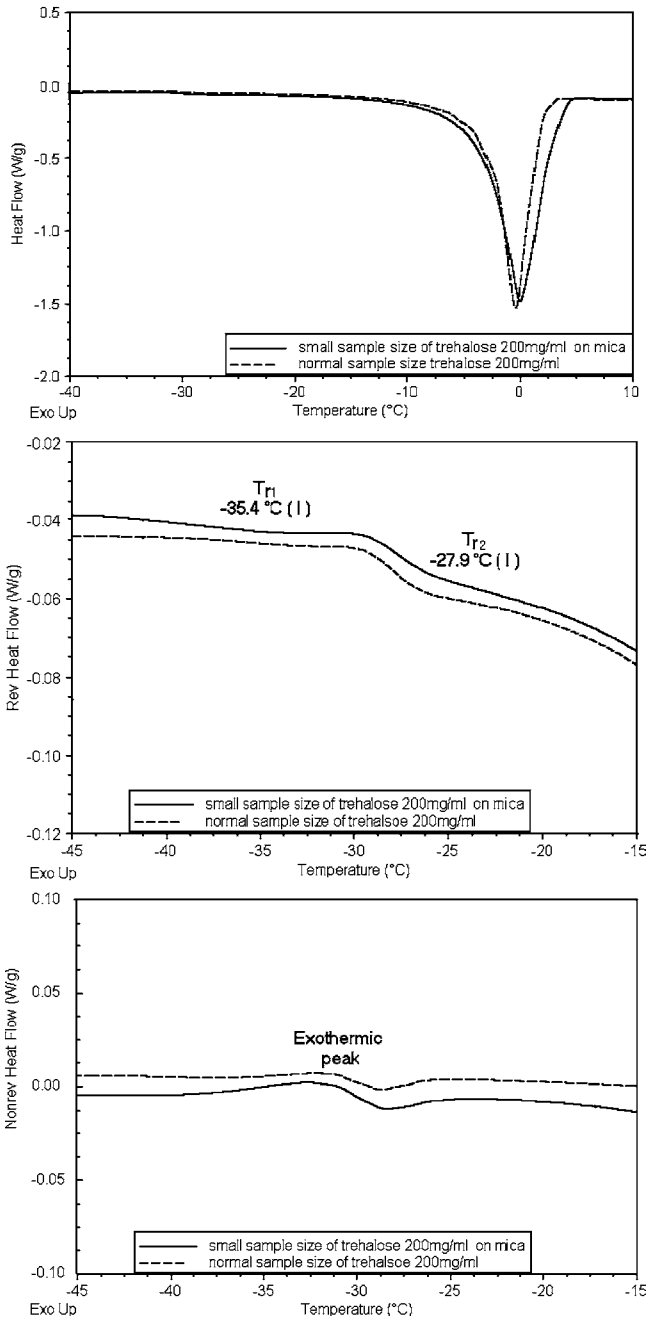

Fig. 1. The heat flow, reverse heat flow and non-reverse heat flow signals of MTDSC results of trehalose 200 mg/ml for small sample size (approximately 2 ml) on mica and normal sample size (approximately 15 ml).

crystals that disappeared at lower temperatures. This was unavoidable without changing the capabilities of the AFM, however, this is fortuitous because this is the fraction of the population that we are most interested in. The importance of this point is further discussed below. In Fig. 2 there is a series of topographic images obtained in contact mode at the temperatures indicated on the MTDSC curve in Fig. 1. It is reasonable to suggest that the raised objects correspond to ice crystals; this is based on the fact that the MTDSC data clearly show a large endotherm that indicates that ice is present (see above). Using the baseline construction proposed by Schawe (15), which simply consists of using a sigmoidal integral construction between the onset of Tr_2 and the offset of the main peak, we estimate the crystallinity to be 89% (expressed as a percentage of total water in the sample). However, it is also worth noting that the crystals are not as angular as might be anticipated; we later present an argument that interprets this observation in terms of there being a layer of amorphous material covering the crystals. Little change in topography is seen through the temperature interval of the lower transition Tr_1 (though a more detailed examination does show subtle but significant changes, see below). When entering the temperature region of the second transition Tr_2, large changes are seen; many, though not all, crystals diminish in size and disappear. These data would therefore strongly suggest that Tr_2 is associated with melting.

In order to further investigate the nature of Tr_1, the surface mechanical properties were examined. These measurements were performed because glass transitions give rise to significant changes in mechanical properties which it was anticipated might be detected using the cryo-AFM. In order to ascertain this we employed force modulation imaging over the range of the lower temperature transition Tr_1; the shading represents the resistance to tip contact pressure and penetration, with darker shades representing more mechanically compliant (soft) regions. The results are shown in Fig. 3, with accompanying topographic images included for comparison. It can be seen that there is a generalised darkening of the surface of the sample with increasing temperature in the force modulation studies and this translates to a softening when entering the temperature region of the first transition; this is therefore compatible with the system undergoing a glass transition. However, considerable care is required when interpreting these images in detail as they contain a number of artefacts. For example, the topography images at −34 and −30°C show some horizontal lines or 'streaking' which suggests that damage is occurring to the sample; this is to be anticipated as force modulation necessarily applies more stress to the sample than contact mode with minimum force. We can also observe that in the amplitude images, at lower temperatures, the right hand side of the edges of the raised features show a consistent apparent high modulus (light appearance). Greater resistance to penetration at edges can be ascribed to the side of the tip rubbing against the side of the raised feature thus giving rise to friction effects as well as substantially increasing the contact area (and so the resistance to penetration). The fact that it occurs on only one side can be attributed to the cantilever being slightly twisted. Such topography-related effects are common in AFM images and can greatly complicate interpretation.

Despite these complications, the data contain several significant features and some analysis is possible. Four regions, two in the flat areas between the raised features (which are free from artefacts at all temperatures) and two on the top of larger raised features (where artefacts, though present, are minimised) were selected (highlighted in Fig. 3 as A, B, C, D). A pixel intensity histogram for a 5 μm × 5 μm area is constructed and fitted to a Gaussian curve (Fig. 4a). As we have previously shown (35), Gaussian behaviour is expected for a pure phase and hence one may calculate mean values and standard deviations for each distribution and use these as an indication of surface mechanical properties as a

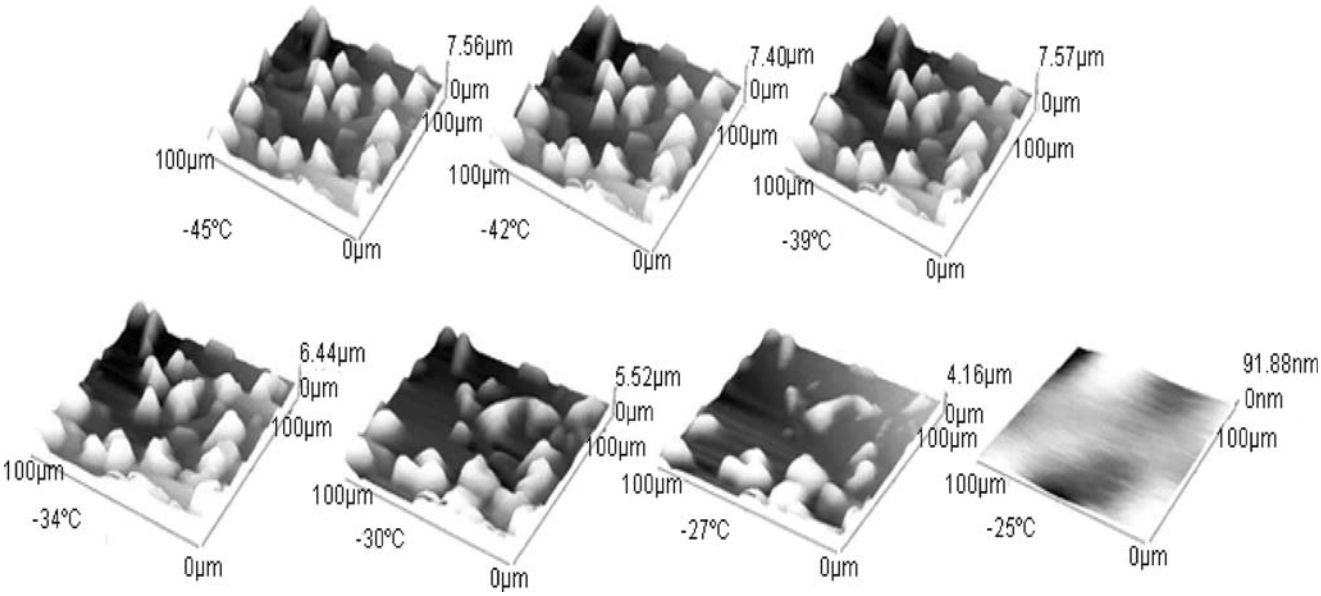

Fig. 2. Topography images from contact mode cold stage AFM over the relevant temperature range.

function of temperature; these are plotted in Fig. 4b. This plot indicates there is a significant drop in resistance to the probe indentation (i.e. a softening of the surface), as the temperature goes above −42°C and into the first transition. This indicates that this is a glass transition and those materials distributed both in between (such as areas A and C) and on top of the raised features (such as areas B and D) undergo this transition. If the top of the crystals and the space between them behave in the same way, this suggests the whole surface is coated with amorphous material. It is possible to obtain the total volume of the raised feature by integrating the heights of all of the pixels in an image and Fig. 4b shows how this volume changes with temperature. There is an apparent decrease in the region of the first transition, a small increase then a dramatic decrease. The decrease in total volume of crystals in the temperature region of the first transition is probably associated with the tip penetrating the now softer amorphous material covering the crystals thus leading to an apparent decrease in size. The subsequent decrease in crystal volume is consistent with the DMA results. We note that there is no indication that crystalline trehalose was formed at any point and we take this to be the case in our discussion.

The DMA results in Fig. 5 show two low temperature transitions in the tan delta curve that are broader that those seen in the MTDSC data, this means they overlap much more, however, the tan delta peak is clearly bimodal and it has been fitted to two Gaussian peaks to aid the interpretation. The complex modulus also shows a two stage reduction in stiffness in this temperature region that supports the AFM observation of a softening starting at approximately −40°C. The onset of the lower temperature transition is also broadly in agreement with the MTDSC reversing signal while the maximum of the higher temperature transition, Tr_2, as seem in tan delta, agrees with that seen in the MTDSC data to within 2°C (i.e. within the experimental error for a DMA experiment) which in turn is in agreement with the second softening event as seen in the complex modulus (it should be remembered that it a strength of our approach to the DMA measurement that the sample is very close to that of the MTDSC experiment because in both cases the sample is encased in a DSC pan). It can be seen (in Fig. 5) from the displacement signal that Tr_2 corresponds to a decrease in thickness (against a background of increasing thickness due to thermal expansion) of the pan-sample composite and this is a strong indication of a volume reduction associated with melting. This is then in agreement with the sharp reduction in the total volume of crystals shown in Fig. 4b. There is then a third stage where there is a peak in tan delta and a step change reduction in complex modulus. This corresponds to the bulk of the loss of crystallinity. The changes are small compared to that observed for the first two transitions as the sample essentially becomes fluid as it passes through the second transition.

Figure 1 shows the non-reversing signal and the small exotherm it exhibits just before the endothermic peak associated with the higher temperature transition; the presence of the exotherm suggests crystallisation is occurring. The images in Fig. 6 show details from the images in Figs. 2 and 3 that illustrate that some of the raised features, most probably ice crystals, increase in size, as might be expected if crystallisation was indeed occurring. Interestingly this is only true of some features; others seem not to change significantly in size. However, the total volumes plot in Fig. 4b shows a net increase in volume after the first transition thus there is net increase in the amount of crystalline material. We can also make the observation that Fig. 5 shows that in between the two softening events seen in the complex modulus, the stiffness increases slightly, this also supports the hypothesis that crystallisation occurs.

When we take all the observations together, the sample softening seen in the force modulation images in the same temperature region as the first step change in the reversing heat capacity and the onset of the first transition in DMA results, this all suggest a glass transition. There is then the increasing size of some crystals and the net increase in crystal volume that accompanies the exotherm in the non reversing

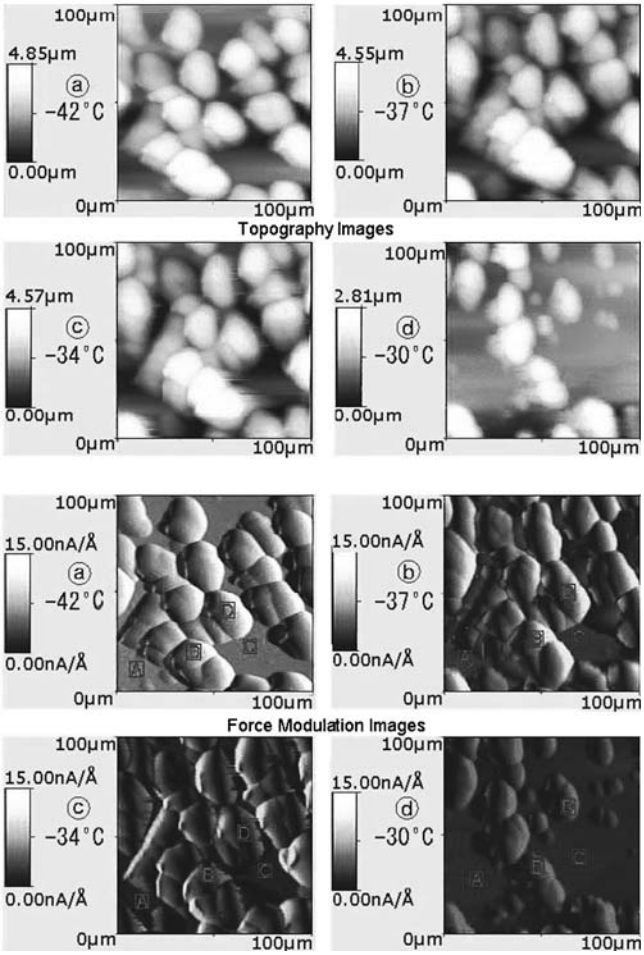

Fig. 3. Topography (*top*) and force modulation (*bottom*) images from temperature −42 to −30°C.

signal as well as the increases in complex modulus, this all strongly supports a model where there is an amorphous phase that goes through its T_g (and this phase is identified by the force modulation experiment) thus enabling some parts of the crystalline phase to increase its size. There is, in fact a remarkable degree of agreement between all of the different measurements on these points and this interpretation is in accordance with other studies that used different methods (36).

The observation that some crystals increase in size invites the question of where the additional water is coming from. If our model is one of a crystalline core surrounded by an amorphous layer then the expectation might be that the amorphous region decreases in volume as the crystalline phase increase as water passes between them. If this occurred simply between an amorphous coating on the crystals and the buried crystalline phase then there might be some small net change in volume as the density of the amorphous phase is different from that of the crystalline. As a guide, the increase in volume when water freezes is about 9% for complete transformation, all of the observed changes are bigger than this. Consequently the water must be able to diffuse to some extent from areas between the raised features after the first transition and it is driven to do so by the thermodynamic driving force of the lower Gibbs free energy of the more crystalline system.

Another aspect of the changing size of the raised features is addressed in Fig. 7. As the temperature traverses the second transition region some features disappear while others remain substantially intact and even grow before disappearing at −25°C. The features near the bottom of the images in Fig. 7 show how the crystals that were seen to grow in Fig. 6 (because the images in Fig. 7 incorporate one of the areas shown in Fig. 6) do not decrease in size while the features near the top, which did not appear to grow in Fig. 6, disappear completely. The images in Fig. 7 contain examples of features which simply reduce in size and disappear (top left), others that remain substantially the same size (bottom left), one example of two features that change size in such a way as to build a bridge between them while overall reducing in size (top right) and another where the features join and increase in size (bottom right). Notwithstanding these interesting details, it is clear from the volume of crystals plot in Fig. 4b and the displacement signal in Fig. 5, that the second transition is associated with a decrease the volume of crystals and so must be associated with the start of the loss of crystallinity.

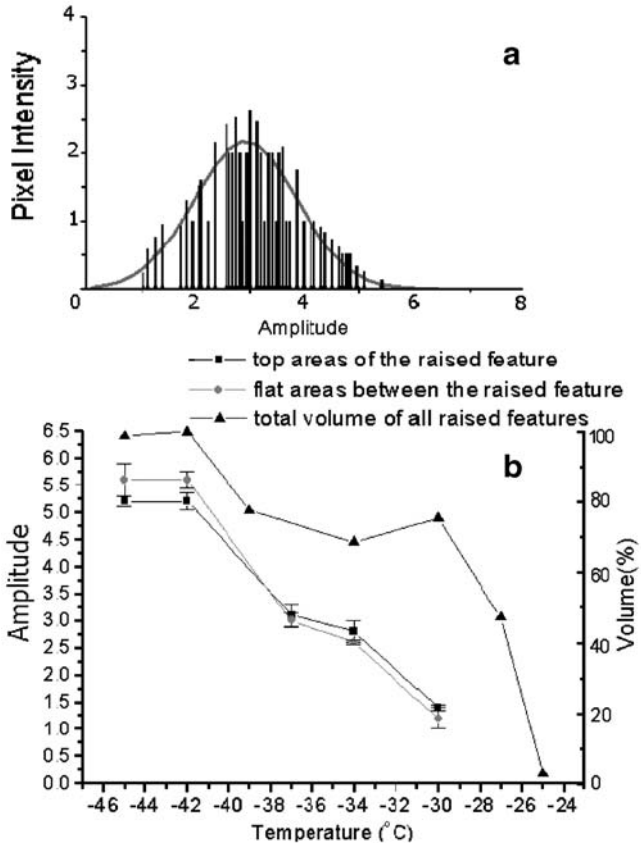

Fig. 4. **a** One example of pixel intensity histogram for the amplitude signal from a force modulation experiment over selected area A together with the Gaussian fit at −37°C. **b** *Left Y axis*: the amplitudes at areas A and C (flat areas between the raised features) and areas B and D (the top of the raised feature); *right Y axis*: total volume of raised features as a function of temperature from contact mode images.

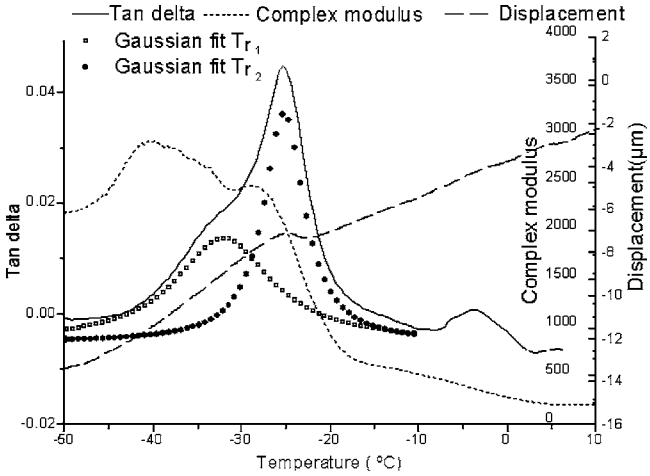

Fig. 5. DMA results, the tan delta signal has been fitted to two Gaussian peaks to make the two transitions clearer. The displacement signal shows how the higher temperature transition is associated with a volume reduction and so it must be predominantly melting.

DISCUSSION

Some consideration must be given to the differences between the MTDSC and the AFM experiments. The former is a bulk measurement on a sample that is about 1 mm thick, the latter is a thin film with a maximum height of approximately 7 μm in the areas that were imaged. Clearly this must have some effect on the behaviour. However the MTDSC results suggest that the two transitions that are the focus of this study are present in both measurements. There is some suggestion that Tr_1 is larger in the mica containing sample but we are not drawing quantitative conclusions as to the amounts of the different phases, we are just seeking to understand the nature of the two transitions. Consequently, there is sufficient similarity between the DSC and (on mica) AFM experiments. An important aspect of the AFM experiment is its inability to look at larger crystals, we conclude that this is why all of the crystals in the field of

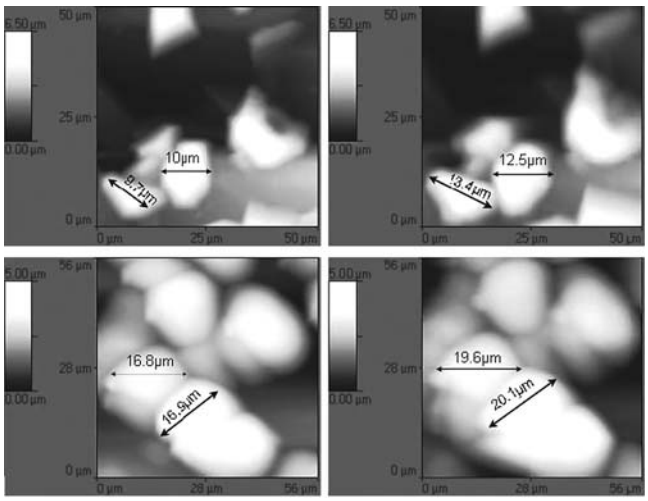

Fig. 6. *Top two images* are topography in contact mode, *left* −45°C, *right* −39°C in same scale. *Bottom two images* are topography on force modulation mode, *left* −42°C, *right* −37°C in same scale.

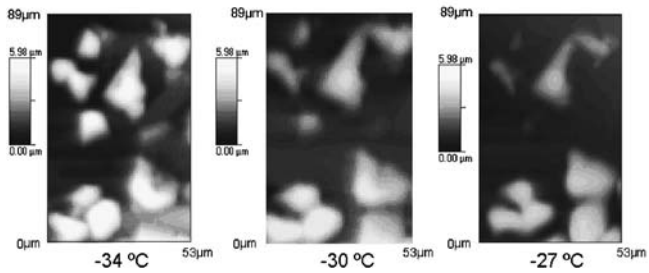

Fig. 7. Detail from Fig. 2 showing structural changes in the temperature region of Tr_2.

vision of the AFM images disappear before the main endotherm, the larger crystals finish decreasing in size at higher temperatures (and this is supported by visual inspection of the optical microscopy that is carried out in parallel with the AFM imaging). It is clear that the softening in the inter-crystal regions is substantially the same as that on the surface of the crystals which suggests we are not dealing with monolayer or close-to monolayer layers between raised features. It must also be recognised that the cooling and heating regimes of the three different experiments were not exactly the same; this was inevitable given the very different measurements being made. It was found that the cooling rate did not greatly affect the MTDSC results (for example cooling at 2°C/min changes the inflection points of the two transitions by only ~1°C compared to rapid cooling). We believe that, these differences not withstanding, the behaviour of the material on the mica is indicative of what is happening in the bulk sample both in the MTDSC and DMA experiments because of the correspondences between the transition temperatures and the observed property and structural changes.

We must also give consideration as to why the polyimide probes proved to be so effective at imaging the sample without damaging it. Of those probes that were tried, the silicon probes that applied the lowest force to the tip had a nominal spring constant of 0.2 n/m, a length of 450 μm, this translates to a higher force than the polyimide probe but by less than a factor of 2, this is unlikely to account for the big difference in observed damage. The diameter of the polyimide probe tip was 100 nm compared to 10 nm for the silicon one; this will certainly have an influence. The silicon probe had 1/4 the width and 2/3 the thickness of the polyimide probe and this tends to reduced thermal transport of the former with respect to the latter, however, the thermal conductivity of the polyimide, at 0.1–0.3 W/mK (37), is 10^3 lower than silicon. It would seem that the combination of the larger tip diameter and much lower thermal conductivity enables the polyimide probe to cause much less damage to the sample as well as providing the very significant additional advantage that it could be used to measure the surface temperature at the point of contact.

Broadly three different types of behaviour are seen in the AFM experiments: there is a softening of the surface in the temperature region associated with the first transition (Tr_1) observed by MTDSC and that observed in the DMA. Some of the raised features increase in size during this temperature interval leading to a net increase in crystal volume and this is probably associated with the exotherm seen in the non-reversing signal shown in Fig. 1 as well as the

slight increase in complex modulus seen in Fig. 5. Finally, as the temperature traverses the region of the second transition, some of the raised features diminish greatly in size before disappearing altogether after Tr_2 while others do not vanish until near the end of this region and some of these even change shape and grow before eventually disappearing at −25°C. The DMA shows this transition is associated with a reduction in overall volume and so an overall decrease in the volume of crystals in the sample.

This observation of heterogeneous behaviour for ice crystals growing and diminishing in size is inconsistent with the classical picture of how this system should behave. It is expected that it will produce pure ice as the system cools within a liquid phase of uniform concentration, this process will reverse on heating. However, the system is clearly metastable (i.e. not at equilibrium) as evidenced by the crystallisation behaviour. This allows for the possibility of an inhomogeneous distribution of trehalose in the amorphous phase with some areas being further from equilibrium than others, this, in turn, allows for the possibility that different parts of the system will behave in different ways. On reheating the amorphous material will go through a glass transition rendering it fluid, further crystallisation might occur, as it is thermodynamically favoured, however, it might not occur for kinetic reasons. In this model it must be assumed that the diffusion within the amorphous matrix is slow, otherwise local differences in concentration would quickly disappear. There are two observations which seem not to be in accordance this explanation of why changes in crystal sizes are inhomogeneous, the first is that the force modulation images suggest homogeneous glass transition behaviour (which would not be the case if the concentration of trehalose were different in different locations), the second is that the fact crystallisation does occur suggests that there is mobility within the amorphous phase. We tentatively suggest a possible alternative; while the process of crystallisation does tend to form pure crystals, in reality this is not a perfect process and impurities can remain. These impurities within the ice might also contribute to the inhomogeneous behaviour. To address this question some form of chemical microscopy is needed, one possibility is Raman microscopy another is photothermal IR spectroscopy (25). This will be the subject of further work.

CONCLUSIONS

The observations made above are broadly consistent with a model in which there are crystalline regions between which there is an amorphous connecting matrix. A substantial amount of the amorphous phase softens at the temperature of the first transition (Tr_1) because this is the glass transition of this phase. Associated with this transition is crystallisation (because this is not a maximally freeze concentrated glass), which can be seen as an exotherm in the non-reversing signal, an increase in the sizes of some crystals and an increase in complex modulus.

As the temperature increases toward the temperature region of the second transition, the volume of crystals decreases, although it happens in an inhomogeneous manner; some features resist disappearing and even change significantly in shape, appearing to grow before finally vanishing. The explanation for this must lie in some form of heterogeneity in the metastability of the system, however, a more detailed understanding will require further work.

In addition to the specific observations we have made on the trehalose solution, the two novel experiments we have developed; the AFM approach that enables soft samples to be imaged even as they undergo glass transitions and melting and the DMA method that enables samples that are liquid at room temperature to be analysed in a configuration similar to that of the DSC (i.e. both are in similarly sized aluminium pans) and also enables data to be gathered on expansion and contraction of the sample. These methods will find application beyond the present study. Aqueous, freeze dried and other systems containing proteinaceous drugs will benefit from examination using these techniques.

ACKNOWLEDGEMENT

We would like to thank Dr Angelo Gaitas for the help of the free test polyimide tips (Picocal Inc., USA).

REFERENCES

1. T. Arakawa, S. J. Prestrelski, W. C. Kenney, and J. F. Carpenter. Factors affecting short-term and long-term stabilities of proteins. *Adv. Drug Deliv. Rev.* **10**:1–28 (1993).
2. J. F. Carpenter, M. J. Pikal, B. S. Chang, and T. W. Randolph. Rational design of stable lyophilized protein formulations: Some practical advice. *Pharm. Res.* **14**:969–975 (1997).
3. L. M. Crowe, R. Mouradian, J. H. Crowe, S. A. Jackson, and C. Womersley. Effect of carbohydrates on membrane stability at low water activities. *Biochim. Biophys. Acta.* **769**:141–150 (1984).
4. J. L. Green and C. A. Angell. Phase relations and vitrification in saccharide-water solutions and the trehalose anomaly. *J. Phys. Chem.* **93**:2880–2882 (1989).
5. B. R. Rudolph, I. Chandrasehar, B. P. Gaber, and M. Nagumo. Molecular modeling of saccharide-lipid interactions. *Chem. Phys. Lipids* **53**:243–261 (1990).
6. D. P. Miller, J. J. Pablo, and H. Corti. Thermophysical properties of trehalose and its concentrated aqueous solutions. *Pharm. Res.* **14**:578–590 (1997).
7. G. M. Wang and A. D. J. Haymet. Trehalose and other sugar solutions at low temperature: Modulated differential scanning calorimetry (MDSC). *J. Phys. Chem. B.* **102**:5341–5347 (1998).
8. P. Bordat, A. Lerbret, J. P. Demaret, F. Affouard, and M. Descamps. Comparative study of trehalose, sucrose and maltose in water solutions by molecular modelling. *Europhys. Lett.* **65**:41–47 (2004).
9. J. H. Crowe, L. M. Crowe, A. E. Oliver, N. Tsvetkova, W. Wolkers, and F. Tablin. The trehalose myth revisited: Introduction to a symposium on stabilization of cells in the dry state. *Cryobiology* **43**:89–105 (2001).
10. A. Lerbret, P. Bordat, F. Affouard, M. Descamps, and F. Migliardo. How homogeneous are the trehalose, maltose, and sucrose water solutions? An insight from molecular dynamics Simulations. *J. Phys. Chem. B.* **109**:11046–11057 (2005).
11. F. Franks. Freeze Drying: From Empiricism to Predictability. *Cryo-Lett.* **11**:93, 1990 (1990).
12. E. Y. Shalaev, and F. Franks. Structural glass transitions and thermophysical processes in amorphous carbohydrates and their supersaturated solutions. *J. Chem. Soc. Faraday Trans.* **91**:1511–1517 (1995).
13. S. Ablett, A. H. Clark, M. J. Izzard, and J. L. Peter. Modelling of heat capacity-temperature data for sucrose-water. *J. Chem. Soc. Faraday Trans.* **88**:795–802 (1992).

14. M. J. Izzard, S. Ablett, P. J. Lillford, V. L. Hill, and I. F. Groves. A modulated differential scanning calorimetric study—Glass transitions occurring in sucrose solutions. *J. Therm. Anal.* **47**:1407–1418 (1996).
15. J. E. K. Schawe. A quantitative DSC analysis of the metastable phase behavior of the sucrose-water system. *Thermochim. Acta.* **451**:115–125 (2006).
16. S. A. Knopp, S. Chongprasert, and S. L. Nail. The relationship between type TMDSC curve of frozen sucrose solutions and collapse during freeze-drying. *Food Sci. Pharmacol.* **54**:659–672 (1998).
17. H. D. Goff, E. V. Verespej, and D. Jermann. Glass transitions in frozen sucrose solutions are influenced by solute inclusions within ice crystals. *Thermochim. Acta.* **399**:43–55 (2003).
18. A. Pyne, R. Surana, and R. Suryanarayanan. Enthalpic relaxation in frozen aqueous trehalose solutions. *Thermochim. Acta.* **405**:225–234 (2003).
19. B. Luyet, and D. Rasmussen. Study by differential thermal analysis of temperature instability of rapidly cooled solutions of glycerol, ethylene glycol, sucrose and glucose. *Biodynamica.* **10**:167–191 (1968).
20. L. Chang, N. Milton, D. Rigsbee, D. S. Mishra, X. Tang, L. C. Thomas, and M. J. Pikal. Using modulated DSC to investigate the origin of multiple thermal transitions in frozen 10% sucrose solutions. *Thermochim. Acta.* **444**:141–147 (2006).
21. M. J. Pikal, and S. R. Shah. The collapse temperature in freeze drying: Dependence on measurement methodology and rate of water removal from the glassy phase. *Int. J. Pharm.* **62**:165–186 (1990).
22. M. Reading, D. Elliott, and V. L. Hill. A new approach to the calorimetric investigation of physical and chemical transitions. *J. Therm. Anal.* **40**:949–955 (1993).
23. M. Reading. A comparison of different evaluation methods in modulated-temperature DSC—Comments. *Thermochim. Acta.* **292**:179–187 (1997).
24. D. Q. M. Craig, and P. G. Royall. The use of modulated temperature DSC for the study of pharmaceutical systems: Potential uses and limitations. *Pharm. Res.* **15**:1152–1153 (1998).
25. H. M. Pollock, and A. Hammiche. Micro-thermal analysis: techniques and applications. *J. Phys. D: Appl. Phys.* **34**:R23–R53 (2001).
26. W. Han, J. Mou, J. Sheng, J. Yang, and Z. Shao. Cryo atomic force microscopy: A new approach for biological imaging at high resolution. *Biochemistry* **34**:8215–8220 (1995).
27. K. Nakamoto, C. B. Mooney, and M. Iwatsuki. Development of low-temperature and high vacuum atomic force microscope with freeze-fracture function. *Rev. Sci. Instrum.* **72**:1445–1448 (2001).
28. S. Zepeda, Y. Yeh, and A. Noy. Determination of energy barriers for intermolecular interactions by variable temperature dynamic force spectroscopy. *Langmuir.* **19**:1457–1461 (2003).
29. Z. Shao, and Y. Zhang. Biological cryo atomic force microscopy: A brief review. *Ultramicroscopy* **66**:141–152 (1996).
30. Z. Shao, D. Shi, and A. V. Somlyo. Cryoatomic force microscopy of filamentous actin. *Biophys. J.* **78**:950–958 (2000).
31. D. Yamamoto, K. Tani, T. Gotoh, and T. Kouyama. Direct observations of freeze-etching processes of ice-embedded biomembranes by atomic force microscopy. *Micron.* **34**:9–18 (2003).
32. M. Reading. Thermomechanical, dynamic mechanical and associated methods. In P. J. Haines P. J. Haines (ed)., *Thermal Methods of Analysis: Principles, Applications and Problems*, Blackie, Glasgow, 1995, pp. 123–160.
33. I. B. Cruz, J. C. Oliveira, and W. M. MacInnes. Dynamic mechanical thermal analysis of aqueous sugar solutions containing fructose, glucose, sucrose,maltose and lactose. *Int. J Food Sci. Technol.* **36**:539–550 (2001).
34. A Gaitas. Polyimide probes for contact-model SPM subsurface thermal imaging applications. *Microscopy and Analysis Suppl* **3**:11–14 (2006).
35. D. B. Grandy, D. J. Hourston, D. M. Price, M. Reading, G. G. Silva, M. Song, and P. A. Sykes. Microthermal characterization of segmented polyurethane elastomers and a polystyrene-poly (methyl methacrylate) polymer blend using variable-temperature pulsed force mode atomic force microscopy. *Macromolecules* **33**:9348–9359 (2000).
36. S. Ablett, C. J. Clarke, M. J. Izzard, and D. R. Martin. Relationship between ice recrystallisation rates and the glass transition in frozen sugar solutions. *J. Sci. Food Agric.* **82**:1855–1859 (2002).
37. H. Yokoyama. Thermal conductivity of polyimide film at cryogenic temperature. *Cryogenics* **35**:799–800 (1995).